Contrib Mineral Petrol
DOI 10.1007/s00410-011-0635-2

ORIGINAL PAPER

Toward a quantitative model of metamorphic nucleation and growth

F. Gaidies · D. R. M. Pattison · C. de Capitani

Received: 5 August 2010 / Accepted: 31 March 2011

Abstract The formation of metamorphic garnet during isobaric heating is simulated on the basis of the classical nucleation and reaction rate theories and Gibbs free energy dissipation in a multi-component model system. The relative influences are studied of interfacial energy, chemical mobility at the surface of garnet clusters, heating rate and pressure on interface-controlled garnet nucleation and growth kinetics. It is found that the interfacial energy controls the departure from equilibrium required to nucleate garnet if attachment and detachment processes at the surface of garnet limit the overall crystallization rate. The interfacial energy for nucleation of garnet in a metapelite of the aureole of the Nelson Batholith, BC, is estimated to range between 0.03 and 0.3 J/m^2 at a pressure of ca. 3,500 bar. This corresponds to a thermal overstep of the garnet-forming reaction of ca. 30°C. The influence of the heating rate on thermal overstepping is negligible. A significant feedback is predicted between chemical fractionation associated with garnet formation and the kinetics of nucleation and crystal growth of garnet giving rise to its lognormal—shaped crystal size distribution.

Communicated by J. Hoefs.

F. Gaidies (✉)
Department of Earth Sciences, Carleton University,
Ottawa, ON, Canada
e-mail: fgaidies@earthsci.carleton.ca

D. R. M. Pattison
Department of Geosciences, University of Calgary,
Calgary, AB, Canada

C. de Capitani
Department of Geosciences, University of Basel,
Basel, Switzerland

Keywords Nucleation · Crystal growth · Interfacial energy · Chemical diffusion · Heating rate · CSD

Introduction

It is generally assumed that the product of a chemical reaction in a rock forms if the formation of that phase lowers the Gibbs free energy of the effective chemical system. However, even when that phase is part of the thermodynamically stable phase assemblage, it may not necessarily nucleate. A departure from equilibrium is required to gain energy for the formation of the interface between reactants and products. This energy is referred to as interfacial energy (e.g., Gibbs 1928; Kaischew and Stranski 1934; Volmer and Weber 1926). It is a function of the structural differences between reactants and products and considered exceedingly small compared to the energies that are released during mineral reactions. In addition to this energy that has to be provided to start mineral reactions in a rock, element transport between the sites of reactant dissolution and product nucleation as well as attachment and detachment processes at the surfaces of the new particles have to be efficient for a mineral reaction to proceed. If the surface processes are sluggish compared to the rates of element transport, gradients in chemical potentials across the interface may form controlling the overall reaction rate (e.g., Kretz 1974; Lasaga 1998). Such a scenario is referred to as interface-controlled and may be envisaged for rocks where element transport rates are assumed to be comparatively fast through the bulk system. If, however, attachment and detachment processes at the interface are faster than element transport rates, gradients in the respective chemical potentials may evolve through the bulk of the system driving crystallization (Carlson

Published online: 21 April 2011

1989). As pointed out by Kelton (2000), a transport-controlled reaction mechanism may not only form depletion zones surrounding product crystals (e.g., Carlson 1991; Carlson et al. 1995; Spear and Daniel 1998) but may also enhance the concentration of product-forming elements in the vicinity of product clusters smaller than nuclei.

In this contribution, we use a simple numerical modeling approach that drops the assumption of chemical equilibrium during crystallization. Instead, it accounts for the departure from equilibrium required for interface-controlled nucleation and growth. We simulate interface processes during isobaric metamorphic mineral reactions by which nuclei and crystals of garnet form on a molecular level based on classical nucleation and reaction rate theory (Becker and Döring 1935; Turnbull and Fisher 1949; Kelton et al. 1983; Lasaga 1998) and Gibbs free energy dissipation in a multi-component system (Hillert 2008; Thompson and Spaepen 1983). Metapelitic garnet is chosen in our study (1) because of its outstanding importance for the determination of metamorphic pressure (P)—temperature (T)—time (t) trajectories (e.g., Spear 1993) and (2) since its specific attenuation properties allow it to be easily detected in metapelites through X-ray computed tomography (Denison et al. 1997). The latter is required in order to study the three-dimensional spatial, size, and abundance distribution of garnet that may provide insights into its crystallization kinetics (e.g., Cashman and Ferry 1988; Kretz 1993; Denison and Carlson 1997).

The crystallization model presented in this paper is based on the inherently interface-controlled classical nucleation theory (CNT) (e.g., Christian 1975; Gibbs 1928; Turnbull 1950; Turnbull and Fisher 1949; Volmer and Weber 1926). Despite its success to describe nucleation in liquids and glasses (e.g., Kelton 1991; Vehkamäki 2006), limitations of CNT can be expected when applied to solid-state crystallization in multi-component systems where elastic strain energy and long-range element transport may influence reaction kinetics. Additional simplifications include a simple nucleus geometry, an isotropic interfacial energy, a well-defined matrix-product interface, and nucleation from a homogenous matrix. In spite of the intrinsic simplifications of CNT, the implementation of this model allows to explore the interplay of several key parameters that impact on crystallization kinetics during petrogenesis. We use our model as a first step toward a more realistic treatment of metamorphic nucleation and growth and discuss the relative influences of interfacial energy and interface mobility on mineral chemistry, mineralogy, and rock texture for different rates of $P-T$ changes during crystallization. We compare the predictions of our numerical experiments to analytical data obtained through X-ray computed tomography and electron-probe micro-analysis and derive relations that may help predicting the departure from equilibrium required for crystallization during geological processes.

The rock sample

The rock sample investigated in this study (sample 93CW4 of Pattison and Tinkham 2009) is a metapelite from the contact aureole of the Nelson Batholith, British Columbia (Pattison and Vogl 2005). Fine-grained biotite, muscovite, and ilmenite form the main foliation of the rock and along with quartz, plagioclase, and idioblastic garnet are the most abundant minerals of the rock. Aligned ilmenite inclusions in the garnet porphyroblasts are interpreted as a former foliation rotated against the foliation of the rock matrix. Rock sample 93CW4 is assumed to have been experienced metamorphic peak conditions of ca. 3.5 kbar and 560°C (Pattison and Tinkham 2009) during contact metamorphism associated with the emplacement of the 159–173 Ma Nelson batholith (e.g., Sevigny and Parrish 1993; Ghosh 1995; Tomkins and Pattison 2007). The apparently random spatial distribution and concentric chemical zoning of the idioblastic garnet crystals in 93CW4 (Figs. 1, 2, 3 of this study and Fig. 5 of Pattison and Tinkham (2009)) may indicate an interface-controlled crystallization mechanism. However, it is important to note that a detailed statistical analysis of the spatial disposition of garnet is required to estimate its crystallization mechanism (e.g., Carlson 2011). On the basis of the sequence and spacing of mineral isograds in the aureole, mineral textures and chemical compositions as well as phase equilibria and thermal modeling, Pattison and Tinkham (2009) suggest an overstepping of up to 30°C for the onset of garnet crystallization in the Nelson aureole. Even though 93CW4 is from the staurolite zone of the contact aureole, it does not contain staurolite as chlorite needed for staurolite growth is assumed to have been used up for garnet formation. For detailed information on the geographical and geological setting, the reader is referred to Pattison and Vogl (2005) and Pattison and Tinkham (2009).

Analytical techniques

WDXRFA

The bulk chemical composition of 93CW4 was obtained through wavelength-dispersive X-ray fluorescence analysis (WDXRFA) on a glass disc using a Philips PW 2400 instrument at the University of Lausanne, Switzerland. About 1 kg of the rock sample, devoid of macroscopically detectable chemical inhomogeneity, was crushed and ground to prepare the rock powder for the fused pellet.

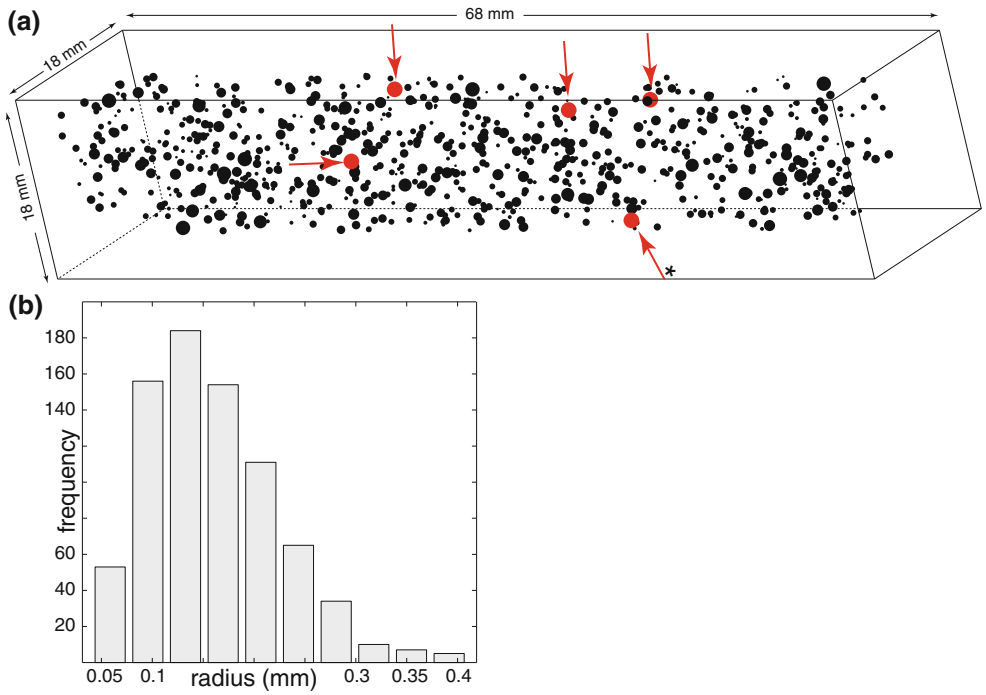

Fig. 1 Size, abundance and spatial distribution of garnet in a cylinder (18 mm × 68 mm) of sample 93CW4 (Pattison and Tinkham 2009) obtained through XR-μ-CT. Garnet crystal shapes are approximated by spheres. The relative size differences between the spheres correspond to the observed garnet crystal size relations. **a** *Arrows* refer to the five biggest crystals of the evenly distributed garnet population (ca. 0.4 mm in radius). The ★ marks the garnet crystal analysed by EPMA (Figs. 2 and 3). **b** Crystal size frequency distribution (CSD) of garnet in the rock cylinder

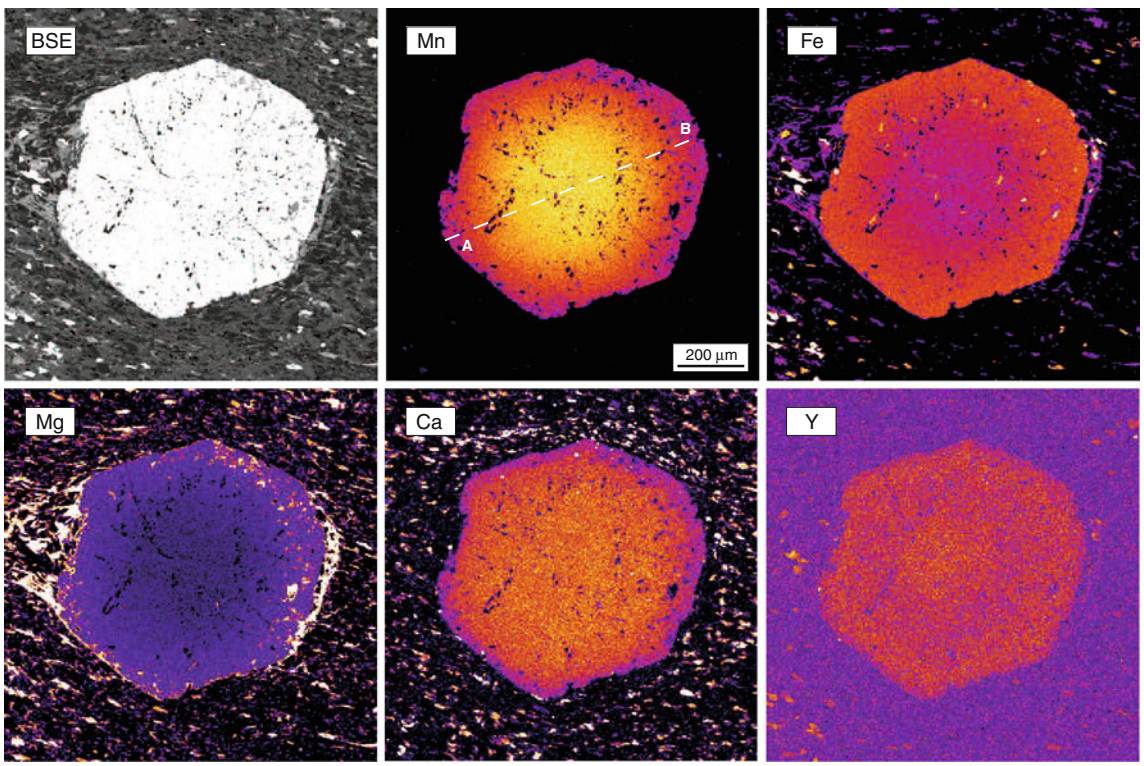

Fig. 2 X-ray maps for Mn, Fe, Mg, Ca, Y and back-scattered electron (BSE) image of the biggest garnet crystal in the cylinder of 93CW4 (marked with a ★ in Fig. 1a). Profile A-B of Fig. 3 is indicated

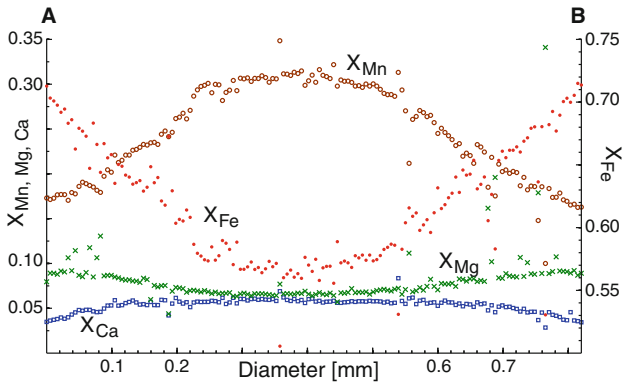

Fig. 3 Compositional profile A-B (see Fig. 2) through the geometric core of the biggest garnet crystal of the cylinder of 93CW4 (marked with a ★ in Fig. 1a)

Table 1 compares the bulk rock composition of 93CW4 to the average Nelson whole-rock composition of Pattison and Vogl (2005) used by Pattison and Tinkham (2009) for phase diagram modeling. The chemical composition of 93CW4 has a lower Mg/(Mg+Fe) ratio (0.38 vs. 0.42) and higher Mn content (0.14 vs. 0.08 wt-%), respectively, compared to the average Nelson bulk composition. The bulk composition of 93CW4 is used in this study to predict the initial equilibrium phase relations and chemical driving forces for garnet nucleation. To model subsequent stages of garnet crystallization, the bulk rock composition was modified numerically to account for element transport across the garnet-matrix interface and fractionation associated with garnet growth (Sect. "Simulations of nucleation and growth of metamorphic garnet").

XR-μ-CT

The size, abundance, and spatial distribution of garnet crystals in 93CW4 (Fig. 1) were studied by X-ray micro-computed tomography (XR-μ-CT). A cylinder with a diameter of 18 mm and a length of 68 mm was cored from the sample and analysed with a SkyScan 1072 tomography scanner at the University of Lausanne, Switzerland. The CT scan was carried out using a 80 kV/ 124 nA X-ray source and a 1-mm-thick Al filter. The cylinder was rotated in the beam over 360° in 0.225° steps. Two-dimensional (2D) attenuation data (slices) were collected and rendered into a three-dimensional (3D) image using SkyScan software (cone-beam reconstruction, version 2.5). The thickness of each slice was 17.81 µm defining a spatial resolution of the 3D image of 17.81 µm per voxel. The digital image processing software Blob3D (Ketcham 2005) was used to quantify the size, abundance, and spatial distribution of garnet. The 3D image was also used to locate the geometrically central cut through the biggest crystal of the rock cylinder (garnet crystal marked with a ★ in Fig. 1a). This central cut was investigated by EPMA (see Figs. 2 and 3).

EPMA

Electron probe micro-analysis was performed on a section through the geometric core of the garnet crystal marked with a ★ in Fig. 1a. Compositional maps with respect to Fe, Mg, Mn, Ca, and Y (Fig. 2) were obtained on the JEOL JXA-8200 electron microprobe at the University of Calgary with the following setting: focused beam, 15 kV, 500 nA, 100 ms dwell time, and 2-µm pixel size. Quantitative compositional profiles were obtained on the Cameca Camebax MBC at Carleton University by wavelength-dispersive X-ray analysis (WDX). Operating conditions were 15 kV accelerating potential and a beam current of 25 nA. Peak counting times for analysed elements were either 30 s or 60,000 accumulated counts. Yttrium was counted for 40 s. Background measurements were made at 50% peak counting time on each side of the analysed peak. Raw X-ray data were converted to elemental weight % by the Cameca PAP matrix correction program. A representative compositional profile is shown in Fig. 3.

Numerical simulation of nucleation and crystal growth

The classical nucleation theory (CNT) is inherently an interface-limited model (Kelton 1991) and can only be applied to systems where nucleation and crystal growth are controlled by interfacial growth-dissolution mechanisms. We apply CNT in our simulations and approximate crystallization during prograde contact metamorphism by the integration of a series of isothermal nucleation and crystal growth events, which are explained in Sects. "Isothermal nucleation of garnet" and "Isothermal crystal growth of garnet", respectively. In each case, it is assumed that there are no T gradients across the volume of the model system. Section "The chemical driving force for nucleation, and the chemical composition of a nucleus" describes an

Table 1 The average composition of metapelites from the Nelson aureole according to Pattison and Vogl (2005) ("Avg.N") and the bulk rock composition of 93CW4 (wt%)

	SiO_2	TiO_2	Al_2O_3	Fe_2O_3	MnO	MgO	CaO	Na_2O	K_2O	P_2O_5	LOI	$\sum$
Avg.N	60.41	0.93	20.10	6.32	0.08	2.30	1.06	1.53	4.17	0.15	3.09	100.14
93CW4	58.91	1.00	20.77	6.36	0.14	1.98	0.43	0.80	5.21	0.12	3.48	99.19

approach to quantify the chemical driving force for nucleation of garnet, and Sect. "Nucleation and growth during $P-T-x-t$ variations" focuses on simulations of nucleation and growth of garnet along a metamorphic $P-T-x-t$ trajectory.

Isothermal nucleation of garnet

Following CNT, the total Gibbs free energy of formation of a spherical garnet cluster[1] of n molecules, ΔG_n, is given by (e.g., Kelton 1991; Porter and Easterling 1992)

$$\Delta G_n = n\Delta G_V + (36\pi)^{1/3}(\bar{v}n)^{2/3}\sigma \tag{1}$$

where ΔG_V is the chemical driving force for nucleation of garnet per garnet molecule (see Sect. "The chemical driving force for nucleation and the chemical composition of a nucleus"), σ is the isotropic interfacial free energy per unit of interfacial area, and $\bar{v}$ is the volume of a garnet molecule (Fig. 4). $\bar{v}$ and the chemical composition of a garnet molecule are calculated in our simulations as a function of pressure (P), temperature (T), and effective bulk chemical composition (x) using the thermodynamic data of Holland and Powell (1998) and the Gibbs free energy minimization algorithm of de Capitani and Brown (1987). Molecules of garnet from which clusters form in our simulations are formula units with the general proportions $X_3Al_2Si_3O_{12}$.

According to CNT, clusters with a size that maximizes ΔG_n are referred to as nuclei (or critical clusters), and their formation is called nucleation. Since they are associated with a maximum in ΔG_n, garnet nuclei are in unstable equilibrium with the rock matrix (Fig. 4). The number of molecules of a nucleus, $n^\star$, can be found by differentiation of (1) and is given by

$$n^\star = \frac{-32\pi\bar{v}^2\sigma^3}{3(\Delta G_V)^3}, \tag{2}$$

and for a spherical geometry, the radius of a nucleus $r^\star$ is equal to

$$r^\star = \frac{-2\bar{v}\sigma}{\Delta G_V}. \tag{3}$$

The critical energy barrier which has to be overcome to form a nucleus is

$$\Delta G^\star = \frac{16\pi\bar{v}^2\sigma^3}{3(\Delta G_V)^2}. \tag{4}$$

Metamorphic nucleation most likely occurs on heterogeneities such as grain boundaries, dislocations, and cracks that catalyse nucleation by reducing $\Delta G^\star$. For

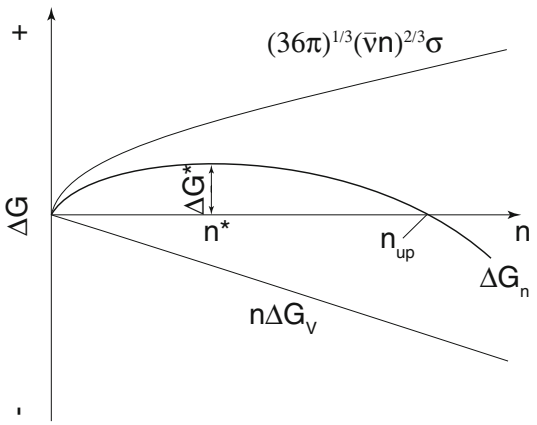

Fig. 4 The Gibbs free energy of cluster formation, ΔG_n, as a function of cluster size, n, incorporating the contributions of the interfacial energy, σ, and the chemical driving force for nucleation, ΔG_V. $\Delta G^\star$ is the critical energy barrier to nucleation, $n^\star$ refers to the number of molecules of a nucleus, and n_{up} is the smallest cluster size considered as crystals in our simulations

nucleation on a planar substrate, the nucleus has the shape of a spherical cap the size of which is determined by the contact angle ϕ between garnet and the rock matrix. In this case, the critical energy barrier is given by (Christian 1975)

$$\Delta G^\star_{het} = \frac{4\pi\bar{v}^2\sigma^3(2+\cos\phi)(1-\cos\phi)^2}{3(\Delta G_V)^2}. \tag{5}$$

Since both σ and ϕ are unconstrained with respect to metamorphic garnet nucleation, we use (4) in our simulations and refer to σ' as the *apparent* interfacial energy. The symbol σ' is used in order to address any reductions in $\Delta G^\star$ that may occur during heterogeneous nucleation. σ' is smaller than σ by a factor

$$f(\phi) = \sqrt[3]{\frac{1}{4}(2+\cos\phi)(1-\cos\phi)^2}. \tag{6}$$

Garnet clusters that are smaller than $n^\star$ shrink in order to lower ΔG_n, and they can only form through random thermal fluctuations. Clusters with $n > n^\star$, however, preferably grow because their formation reduces ΔG_n. CNT predicts that once ΔG_V is negative, a finite number of garnet clusters of various sizes is present, and that smaller ones are more abundant than larger ones (e.g., Christian 1975; Kelton 2006). Clusters of n molecules, E_n, are assumed to shrink or grow by loss or addition of a single molecule, E_1, through a series of bimolecular reactions

$$\begin{aligned} E_{n-1} + E_1 &\underset{k_n^-}{\overset{k_{n-1}^+}{\rightleftarrows}} E_n \\ E_n + E_1 &\underset{k_{n+1}^-}{\overset{k_n^+}{\rightleftarrows}} E_{n+1} \end{aligned} \tag{7}$$

where k_n^+ is the rate with which a molecule is attached to the surface of a cluster of size n, and k_n^- is the rate of

[1] In our simulations, garnet clusters are assumed to be spherical.

detachment of molecules from E_n. Based on reaction rate theory (Turnbull and Fisher 1949) and for a spherical cluster geometry, molecular attachment and detachment rates are approximated in our simulations by

$$k_n^+ = 4n^{2/3}\gamma \exp\left(\frac{-\delta g_n}{2k_BT}\right)$$
$$k_{n+1}^- = 4n^{2/3}\gamma \exp\left(\frac{+\delta g_n}{2k_BT}\right) \quad (8)$$

where $\delta g_n = \Delta G_{n+1} - \Delta G_n$, and k_B is Boltzmann's constant. γ is the molecular jump rate into and out of the garnet cluster surface

$$\gamma = \frac{6D}{\lambda^2} \quad (9)$$

with the jump distance, $\lambda = \bar{v}^{1/3}$, and D, the molecular mobility at the garnet-matrix interface.

Similar to Kubena et al. (2007), we derive the garnet cluster size frequency distribution $N_n(t)$ by solving a modified system of Becker-Döring equations (Becker and Döring 1935; Kelton 1991)

$$\frac{dN_1}{dt} = -\sum_{i=1}^{v-1} k_i^+ N_i + \sum_{i=2}^{v}(k_i^+ + k_i^-)N_i - \sum_{i=3}^{v+1} k_i^- N_i$$
$$\frac{dN_i}{dt} = k_{i-1}^+ N_{i-1} - (k_i^- + k_i^+)N_i + k_{i+1}^- N_{i+1} \quad \text{for} \quad 1 < i < v \quad (10)$$

where $v + 1$ is the upper limit of the range of cluster sizes that are considered in our calculations. The numerical value of v depends on ΔG_V, σ', and $\bar{v}$ and is chosen to represent a cluster size that is bigger than n_{up}, the upper root of the $\Delta G(n)$ function (see expression (1) and Fig. 4). Following Kelton et al. (1983), $N_{n \geq v}(t)$ is taken to be zero to ensure that there is no backward flux of molecules from stable clusters.

Due to the formation of stable garnet clusters, the number of clusters with single molecules $N_1(t)$ available for garnet nucleation decreases with time. The modified system of Becker-Döring equations (10) accounts for the decrease in $N_1(t)$. It represents a numerically stiff set of ordinary differential equations that is solved using the MATLAB solver ode15s (Shampine and Reichelt 1997; Shampine et al. 1999) with the initial conditions (Kelton 2003; Kubena et al. 2007)

$$N_n(0) = \begin{bmatrix} N_1(0) \\ N_2(0) \\ \vdots \\ N_v(0) \end{bmatrix} = \begin{bmatrix} N^{eq} \exp\left[\frac{-\Delta G_V}{k_BT}\right] \\ 0 \\ \vdots \\ 0 \end{bmatrix} \quad (11)$$

where N^{eq} is the number of garnet molecules predicted to form at given $P - T - x$ conditions during thermodynamic equilibrium according to Gibbs free energy minimization (de Capitani and Brown 1987). During each simulation, the number of garnet nuclei $N_{n^\star}(t)$ is monitored and events such as the onset and end of nucleation and crystal growth, respectively, are registered.

Isothermal crystal growth of garnet

Since garnet nuclei are in unstable equilibrium with the rock matrix, they either shrink in our model, if they become subcritical ($n < n^\star$) or grow, if they become supercritical ($n > n^\star$). In our simulations, the supercritical clusters that correspond to the upper root of the $\Delta G(n)$ function (1), $E_{up}(t)$, are considered the smallest crystals (see Fig. 4). Upon their formation, the overall net change in Gibbs free energy, ΔG, is negative compared to the precursor system.

In principle, if crystal growth is continuous and interface-controlled, the bimolecular rate theory applied in (10) may also be valid for the growth of large clusters $E_{n \gg up}(t)$. However, due to finite computer resources, the formation of such clusters is not simulated directly. The biggest garnet crystals that can be considered in our calculations by integration of (10) consist of approximately 2×10^6 molecules, which corresponds to a diameter of ca. 90 nm. The growth rate of bigger crystals is determined analytically through (Kelton and Weinberg 1994)

$$\frac{dr}{dt} = \left(\frac{3\bar{v}}{4\pi}\right)^{1/3} \frac{16D}{\lambda^2} \sinh\left[\frac{\Delta G_V}{2k_BT}\left(1 - \frac{r^\star}{r}\right)\right]. \quad (12)$$

This growth law allows growth of supercritical clusters as well as resorption of subcritical clusters, and thus naturally encompasses so-called coarsening or "Ostwald ripening". For $r \gg r^\star$, radial crystal growth becomes size independent and is only a function of the molecular mobility at the garnet-matrix interface. It is important to note that the volumetric growth rate is size dependent and scales with the surface of garnet for any given crystal size.

The chemical driving force for nucleation and the chemical composition of a nucleus

The chemical driving force for nucleation is given by the maximum volumetric Gibbs free energy difference ΔG_V between reactant and product. In our simulations, the rock matrix is considered to be thermodynamically homogenous with equilibrium properties, and reactions among matrix phases are assumed to take place at equilibrium. The matrix reacts to form garnet clusters once garnet is part of the thermodynamically stable phase assemblage but a certain departure from equilibrium is required for garnet nucleation. Motivated by the approach presented by Thompson and Spaepen (1983) (see also Hillert 1999; Hillert and Rettenmayr 2003; Hillert 2008), but extended to

the multi-component model system MnO–Na_2O–CaO–K_2O–FeO–MgO–Al_2O_3–SiO_2–H_2O–TiO_2 (MnNCKFMASHT), the chemical composition of a garnet nucleus, x_{grt}^{nuc}, is assumed to be the one that maximizes ΔG_V. x_{grt}^{nuc} differs from the equilibrium composition of garnet, x_{grt}^{eq}, at given $P-T-x$ conditions, the difference being dependent on the G-x functions of the garnet solid solution and the phases that form the rock matrix (Fig. 5). Whether garnet eventually approaches x_{grt}^{eq} following nucleation is controlled by the efficiency of chemical diffusion through its volume and across its interface with the rock matrix. Figure 5 illustrates that the differences in chemical potentials of garnet-forming components between the matrix of the rock and the garnet nucleus ($\Delta\mu^A$ and $\Delta\mu^B$ in Fig. 5) are zero. This configuration is required to maximize the Gibbs free energy that dissipates during nucleation, ΔG_V, and is calculated in our simulations based on a modification of the THERIAK algorithm (de Capitani and Brown 1987). A similar approach is used by Pattison et al. (in print) to construct maximum affinity maps for the formation of garnet, staurolite, andalusite, and cordierite relative to a matrix where these phases are absent.

Nucleation and growth during $P-T-x-t$ variations

In this study, we have chosen an isobaric heating scenario in order to model nucleation and growth of garnet during contact metamorphism in the Nelson aureole (Pattison and Vogl 2005; Pattison and Tinkham 2009). Garnet cluster evolution is simulated through a succession of isothermal steps the duration of which is given by a constant heating rate and a temperature step size of 0.1 K. After each isothermal step, the growth law (12) is applied to all new clusters E_{up} and to the garnet crystals previously formed. If garnet does not nucleate but $\Delta G_V < 0$, older crystals may grow or shrink dependent on their sizes relative to $r^\star$. An energy barrier to crystal growth and dissolution is not considered in such a case. As $r^\star$ changes during $P-T-x-t$ evolution, preexisting garnet clusters formerly grown to crystals may become subcritical and subject to resorption. Preexising supercritical clusters will be overgrown by garnet with the composition x_{grt}^{nuc}. Once chemical zoning developed across the volume of a garnet crystal, chemical diffusion within garnet is simulated following the finite differences approach presented by Gaidies et al. (2008) using the kinetic data of Chakraborty and Ganguly (1992). The number of garnet molecules used for crystal growth is subtracted from the bulk system, and the effective bulk composition for the next step is adjusted accordingly in order to account for the effect on ΔG_V of chemical fractionation during garnet growth.

Results

The chemical driving force for garnet nucleation, ΔG_V

Figure 6b illustrates ΔG_V as a function of P and T and on the basis of the bulk rock composition given in Table 1.

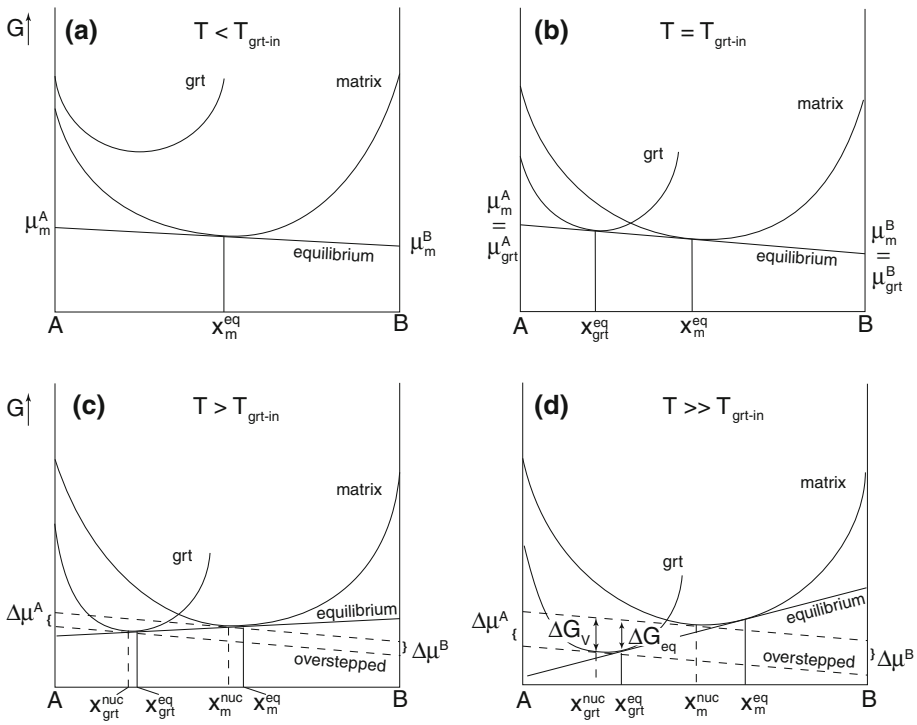

Fig. 5 Series of schematic G-x diagrams illustrating the relationships between ΔG_V and x_{grt}^{nuc} for various degrees of thermal overstepping

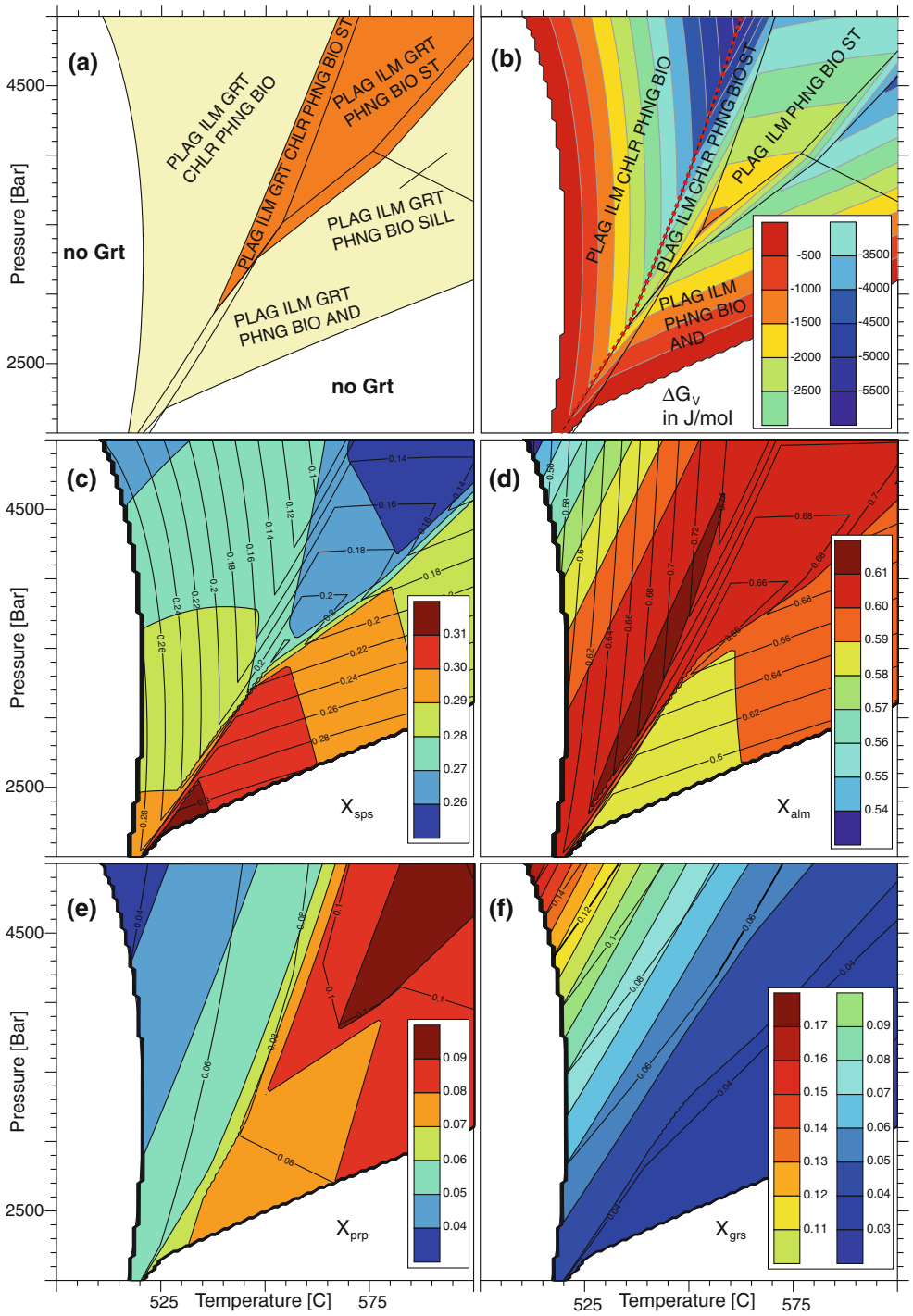

Fig. 6 Relationship between the chemical composition of a garnet nucleus, x_{grt}^{nuc}, and the chemical driving force for its formation, ΔG_V, as a function of P and T calculated for rock sample 93CW4. **a** Equilibrium phase relations for the bulk chemical system given in Table 1 calculated with DOMINO (de Capitani and Petrakakis 2010) using the thermodynamic data of Holland and Powell (1998); all assemblages contain quartz and H_2O; assemblages with staurolite are marked with darker color. For the calculations of (**b**–**f**), the $P-T$ space was scanned along a grid with $\Delta T = 1°C$ and $\Delta P = 50$ bar. ΔG_V and x_{grt}^{nuc} were calculated using the "tangent method" outlined in Sect. "The chemical driving force for nucleation and the chemical composition of a nucleus". **b** The driving force for garnet nucleation reaches maxima at stability limits of matrix phase assemblages with staurolite (marked with *stippled line*). **c**–**f** The difference between x_{grt}^{nuc} (*color-coded*) and x_{grt}^{eq} (contours) increases with departure from the limits of garnet stability. The difference is greater for x_{sps} and x_{alm} than for x_{prp} and x_{grs}

Only those parts of the diagram are color-coded where ΔG_V is negative. Positive areas are omitted because in our model nucleation of garnet at the corresponding $P - T$ conditions is impossible as it would increase the energy state of the system. In general, the chemical driving force increases (ΔG_V becomes more negative) with thermal overstep of the low-T conditions of the garnet stability field and decreases (ΔG_V becomes less negative) toward its high-T limit. It is important to notice the influence of staurolite and andalusite on ΔG_V : The lower T - limits at which staurolite and andalusite enter the equilibrium assemblage are characterized by a "channel" in ΔG_V–$P - T$ space and, thus, mark the $P - T$ conditions with highest garnet nucleation probability (stippled line in Fig. 6b). This indicates that, for a constant σ and during isobaric heating, nucleation of garnet is unlikely once staurolite or andalusite formed.

Similar to the chemical driving force for garnet nucleation, the differences between x_{grt}^{nuc} and x_{grt}^{eq} increase with departure from the stability limits of equilibrium phase assemblages that contain garnet. The differences between x_{grt}^{nuc} and x_{grt}^{eq} are minute with respect to the pyrope and grossular contents but significant for spessartine and almandine (Fig. 6c, d, e, f). The relationships between ΔG_V, x_{grt}^{nuc}, and x_{grt}^{eq} for isobaric heating at 3,500 bar are illustrated in Fig. 7. They show that the largest differences between x_{grt}^{nuc} and x_{grt}^{eq} correlate with maxima in the chemical driving force for garnet nucleation. It is important to note that for the calculations of Figs. 6 and 7, it is assumed that the chemical composition of the thermodynamically effective system does not change during garnet crystallization. In other words, the $P - T - t$—path—dependent influence of chemical fractionation on ΔG_V is not considered. This factor is considered, however, in the simulations outlined below.

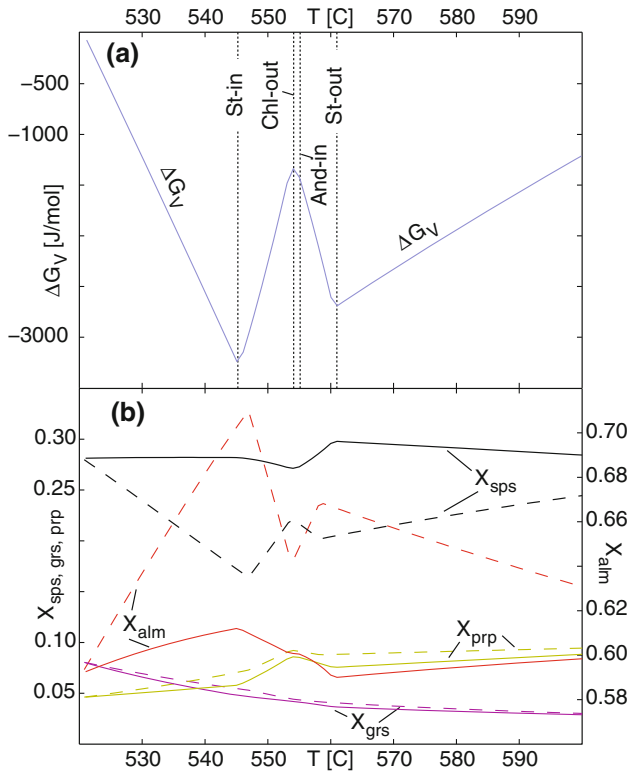

Fig. 7 Relationship between **a** the chemical driving force for garnet nucleation ΔG_V, and **b** the chemical composition of a garnet nucleus, x_{grt}^{nuc} (*unbroken lines*), and the equilibrium composition of garnet, x_{grt}^{eq} (*dashed lines*; calculated with THERIAK (de Capitani and Brown 1987)), for isobaric heating of 93CW4 between 520 and 600°C at 3,500 bar. Calculations are based on the bulk rock composition given in Table 1

Simulations of nucleation and growth of metamorphic garnet

Figure 8a and b illustrate the CSD of garnet and the compositional profile of the largest garnet crystal that we predict to evolve in the cylinder of 93CW4 after isobaric heating at 3,350 bar between 500 and 600°C using a heating rate of 1,000°C/Ma and an apparent interfacial energy, σ', of 0.016 J/m^2. P and heating rate correspond, within error, to the estimates obtained by Pattison and Tinkham (2009). Subject to the simplified treatment of our model, a value of 0.016 J/m^2 for σ' yields the best fit between observed and predicted maximum crystal sizes. Using this set of parameters, garnet is predicted to crystallize between 530.3 and 544.5°C (Fig. 8c, d, e). These simulations imply that a thermal overstep of ca. 10°C is required to nucleate garnet above its predicted entry at ca. 520°C. For this setting, the radius of a nucleus, $r^{\star}$, at the onset of garnet crystallization is predicted to be ca. 2.9 nm. Chemical fractionation associated with garnet growth shifts the lower limit of garnet stability up-T and -P (lines labeled (1), (2) and (3) in Fig. 8c), thus modifying the departure from equilibrium and the chemical driving force for garnet nucleation. The garnet growth rate, dr/dt, decreases slightly before nucleation stops at 531.3°C (Fig. 8e) when the driving force becomes too small to overcome $\Delta G^{\star}$. At $T > 531.3$°C, the garnet population changes solely through crystal growth, and the differences between x_{grt}^{nuc} and x_{grt}^{eq} get smaller (Fig. 8d). At ca. 532.5°C, chemical fractionation decreased the driving force such that differences between x_{grt}^{nuc} and x_{grt}^{eq} become insignificant, and dr/dt is decreased by an order of magnitude. Subsequent growth at low rates up to ca. 544.5°C is responsible for the compositional gradients characteristic for the outermost 0.2-mm-thick garnet rim (Fig. 8b). At ca. 544.5°C, staurolite enters the thermodynamically stable equilibrium assemblage that forms the rock matrix, and ΔG_V becomes positive making further garnet growth impossible (Fig. 8).

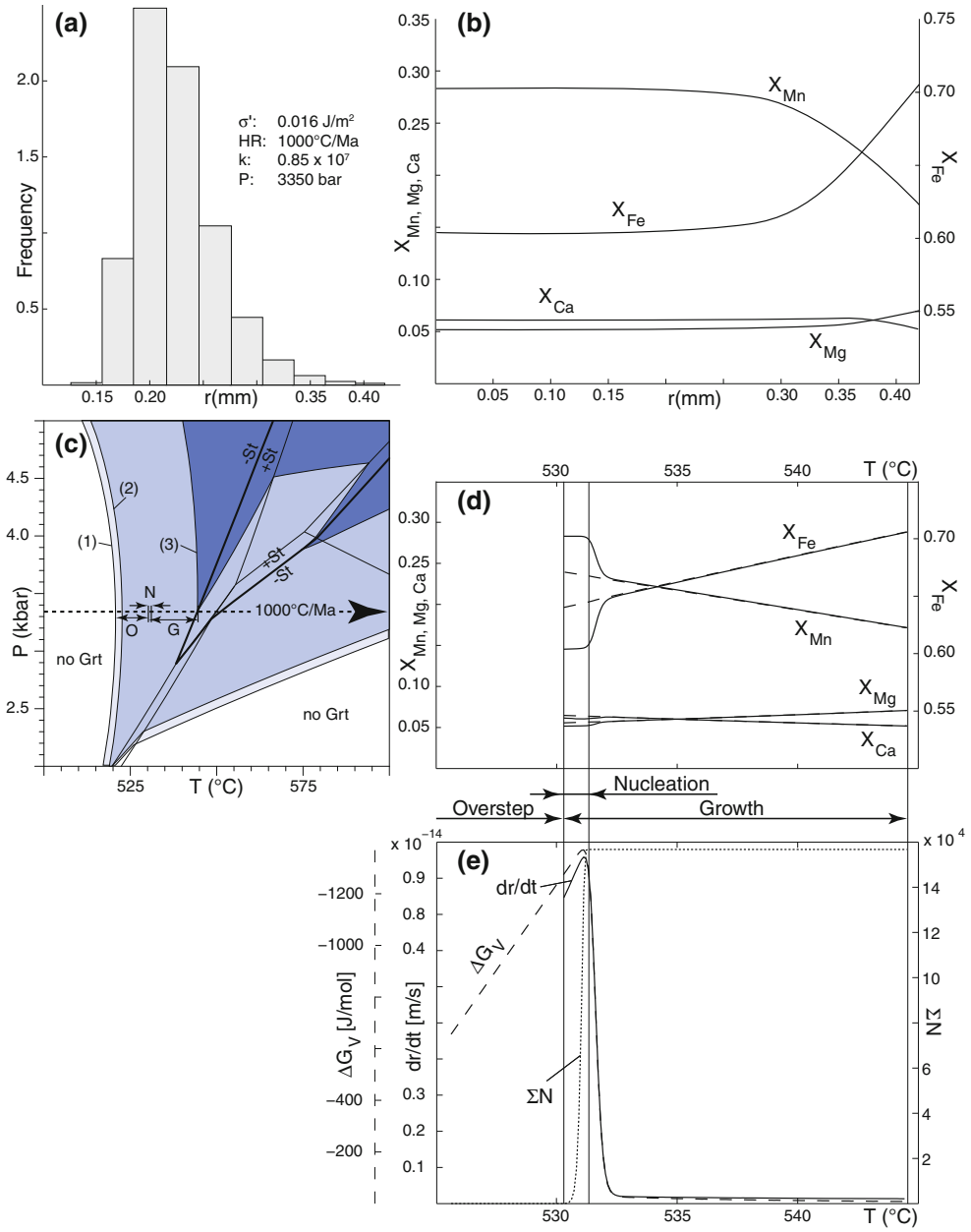

Fig. 8 Predicted garnet CSD and compositional profile of the biggest garnet crystal in the rock cylinder of 93CW4 for $\sigma' = 0.016$ J/m^2; heating rate (HR) = 1,000°C/Ma; k = 0.85 × 10^7; $P = 3{,}350$ bar. **a** Final garnet CSD after isobaric heating; **b** Compositional profile from the center to the rim of the biggest garnet crystal; **c** Locations of the lower limit of garnet stability calculated based on three different effective bulk rock compositions accounting for chemical fractionation during garnet growth: (1) bulk rock composition of 93CW4; (2) effective bulk rock composition directly after nucleation stopped; and (3) effective bulk rock composition after garnet growth stopped; O = thermal overstep, N = T-range of nucleation, G = T-range of growth; P-T-range of assemblages with staurolite is outlined and is the same for all three bulk compositions; **d** Change of garnet composition during isobaric heating; *unbroken lines* correspond to x_{grt}^{nuc}, dashed lines reflect x_{grt}^{eq}; (e) Relationship between ΔG_V, the growth rate of garnet crystals with $r \gg r^{\star}$, dr/dt, and the total number of garnet crystals formed in the cylinder, $\sum N$

Since Ca is the slowest diffusing major component in metapelitic garnet, its mobility at the garnet-matrix interface may limit garnet cluster formation rates. In our simulations, the molecular mobility at the garnet-matrix interface, D, is monitored relative to the tracer diffusion coefficient of Ca in garnet, $D_{Ca}^{\star}$. Following the approach of Loomis et al. (1985) and Florence and Spear (1991), $D_{Ca}^{\star}$ may be approximated by $D_{Ca}^{\star} = 1/2 D_{Fe}^{\star}$. The way D is calculated in our simulations is as follows:

$$D = kD_{Fe}^{\star} = kD_0^{Fe} \exp\left[\frac{-E_a^{Fe} - (P-1)\Delta V_a^{Fe}}{RT}\right] \quad (13)$$

with the proportionality factor k, and the pre-exponential constant D_0^{Fe}, the activation energy E_a^{Fe} and the activation volume ΔV_a^{Fe} taken from Chakraborty and Ganguly (1992). For the calculations illustrated in Fig. 8, $k = 0.85 \times 10^7$ so that D ranges between 5.2×10^{-24} and 1.3×10^{-23}m^2/s during garnet crystallization corresponding to a jump frequency, λ, of ca. 9.2×10^{-5} to 2.3×10^{-4}s^{-1}, respectively.

In the following, we will illustrate the sensitivity of the CSD and chemical composition of garnet to changes in σ', D, P, and heating rate, HR. A discussion of the results follows in Sect. "Discussion".

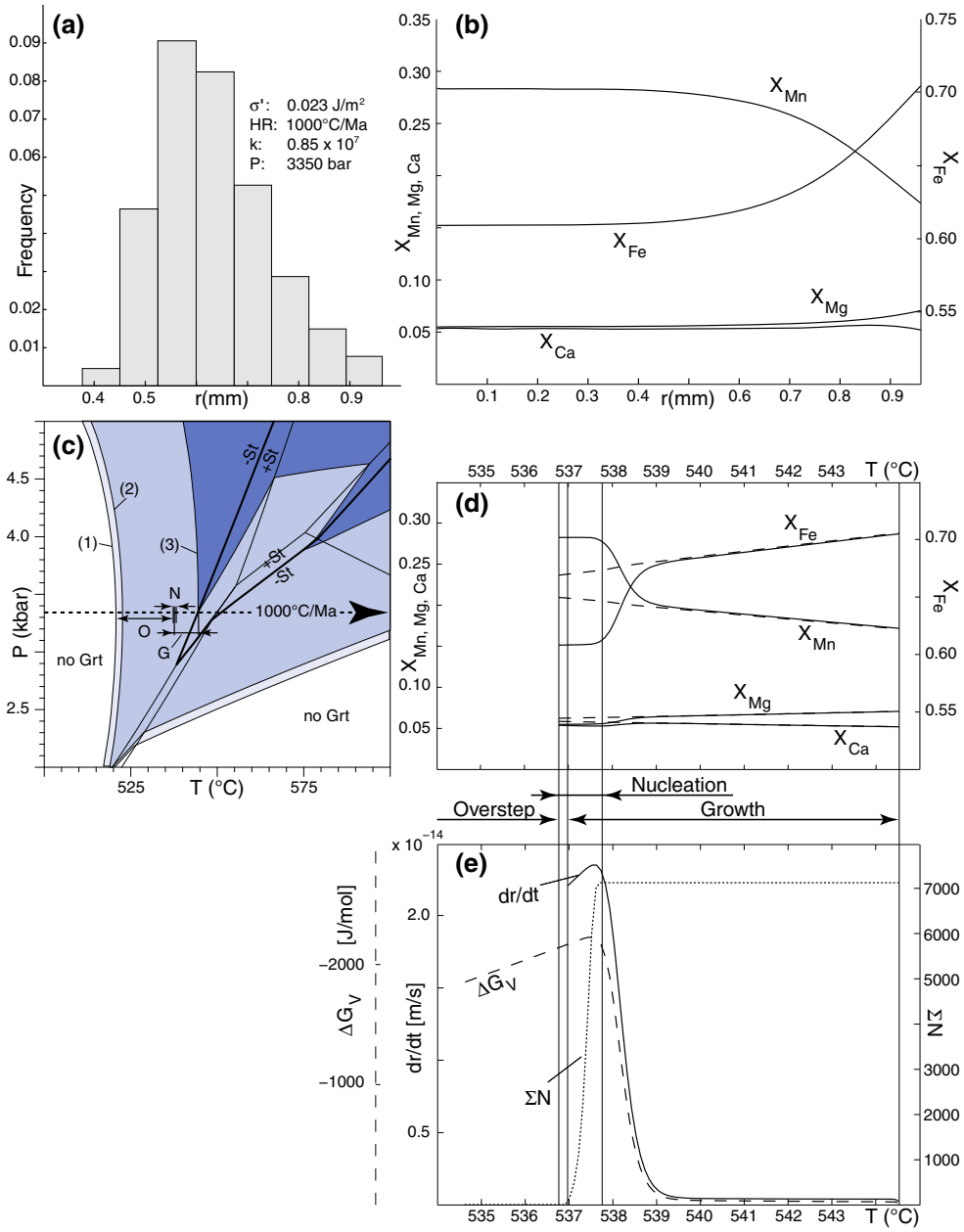

Fig. 9 Like Fig. 8 but with $\sigma' = 0.023$ J/m^2

The apparent interfacial energy, σ'

Compared to the overstep of 10°C for $\sigma' = 0.016$ J/m^2, an overstep of ca. 17°C is required to nucleate garnet if $\sigma' = 0.023$ J/m^2 (Fig. 9c). The chemical composition of the biggest garnet crystal is similar to the case where $\sigma' = 0.016$ J/m^2 (Figs. 8b, 9b). However, the slightly bigger σ' alters the garnet CSD notably. The radii of the largest crystals are bigger by a factor of two, a pattern mimicked by the size range of the entire population. This coincides with a decrease in the number of garnet crystals per rock cylinder (compare Figs. 8a and 9a). Similar to the case where $\sigma' = 0.016$ J/m^2 garnet nucleates over a T-range of ca. 1 to 1.5°C. Changes in phase relations that are associated with chemical fractionation during this T-interval are minor. This is the reason why the core compositions of all garnet crystals are predicted to be similar. As they start to crystallize at negligibly different T conditions but different times along the heating path and stop growing simultaneously at ca. 544 to 545°C their final sizes are different.

At the onset of crystallization, the larger ΔG_V needed to nucleate garnet if $\sigma' = 0.023$ J/m^2 results in smaller nuclei compared to the case where $\sigma' = 0.016$ J/m^2 ($r^{\star}_{\sigma'=0.016} = 2.94$ nm at $T = 530.3$°C, $r^{\star}_{\sigma'=0.023} = 2.48$ nm at $T = 537$°C). However, the larger ΔG_V also speeds up crystal

growth (12) increasing supercritical cluster sizes and shifting the lower limit of garnet stability up-T and P through enhanced chemical fractionation. The resulting decrease in garnet stability decelerates garnet nucleation during subsequent crystallization stages and reduces the maximum number of crystals present in the cylinder by an order of magnitude. It is interesting to note that for $\sigma' = 0.023$ J/m^2 nucleation and growth do not start simultaneously. Only a few hundred years after nucleation started and at a slightly higher T, the cluster population begins to contain crystals E_{up} (Fig. 9d).

The thermal overstep for $\sigma' = 0.01$ J/m^2 is ca. 5.6°C (Fig. 10c). The relatively small ΔG_V prevents fast growth reducing the aforementioned feedback of chemical fractionation into nucleation kinetics. The corresponding garnet CSD is shown in Fig. 10a. It suggests that for the same heating and element transport rates smaller interfacial energies increase crystal frequencies and reduce crystal sizes and population size ranges. It is important to note that as the chemical driving force goes through a maximum during crystallization and eventually approaches zero to stop growth, the radial garnet growth rate, dr/dt, goes through a maximum, too. The decrease in dr/dt after the maximum is accelerated as σ' decreases (compare dr/dt in Figs. 8e, 9e, 10e). The maximum radial growth rate is relatively small for $\sigma' = 0.01$ J/m^2 (Fig. 10e) and almost immediately approaches zero once nucleation stops. The periods at ca. $T > 535$°C where ΔG_V oscillates about zero

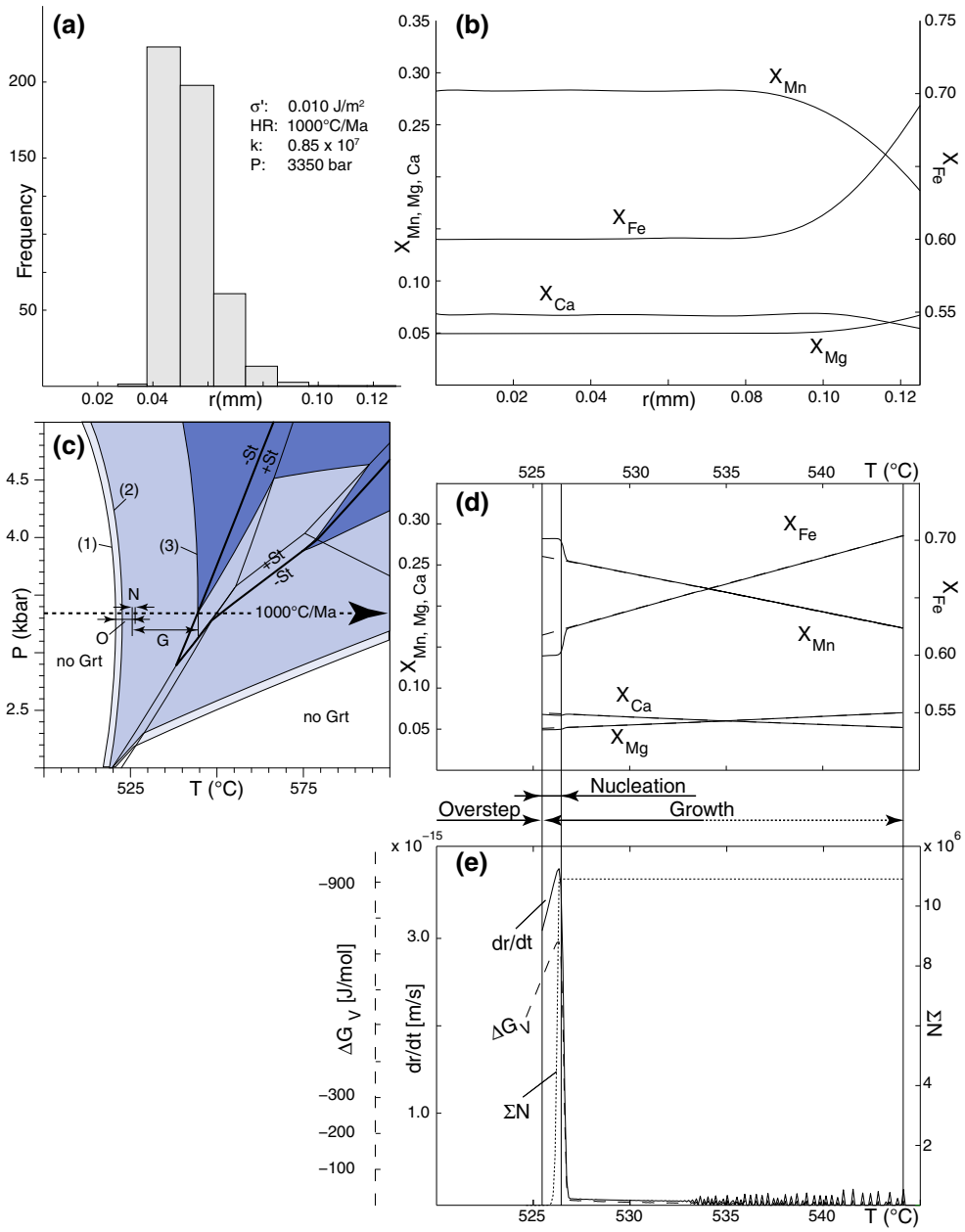

Fig. 10 Like Fig. 8 but with $\sigma' = 0.01$ J/m^2

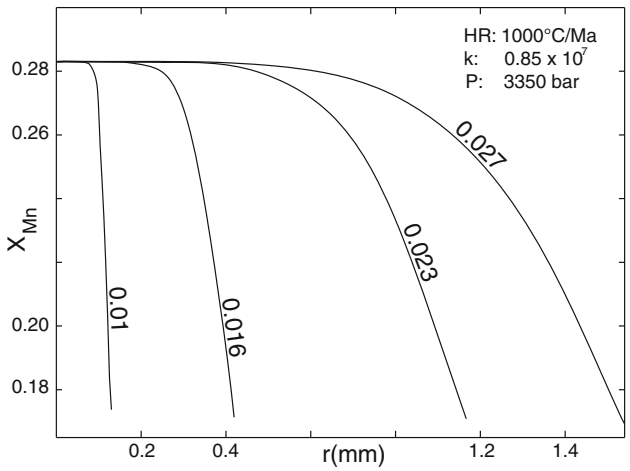

Fig. 11 Distribution of X_{Mn} from core to rim of the biggest garnet crystal predicted for different values of σ' (in J/m^2)

are artifacts of the model that disappear if the isothermal step size is minimized.

Irrespective of its strong influence on garnet CSD, the impact of chemical fractionation during nucleation on equilibrium phase relations is minute. For the three cases explained above ($\sigma' = 0.016$, 0.023, 0.01 J/m^2), the respective shifts of the garnet-in curve up P and T associated with chemical fractionation are similar (line (2) reflects the garnet-in curve after nucleation finished and (3) corresponds to the garnet-in curve once growth stopped, in Figs. 8c, 9c and 10c, respectively). In all cases, garnet crystallization stops at conditions at which staurolite enters the equilibrium matrix assemblage.

Figures 8a, 9a, and 10a illustrate that higher apparent interfacial energies result in larger crystal sizes and population size ranges and smaller crystal frequencies. Using the sps-content of the biggest garnet crystal, Fig. 11 shows that σ' also affects the compositional gradients of garnet. Whereas the decrease in sps-content is restricted to the outermost rim portion of garnet that originates from $\sigma' = 0.01$ J/m^2, larger values of σ' result in bigger volumes of garnet being chemically zoned. In order to investigate the fact that σ' may not be constant but increases as the number of preferred low-energy nucleation sites decreases during crystallization, in the calculations illustrated in Fig. 12, σ' was related to the maximum number of crystals previously formed

$$\sigma'_{i+1} = \sigma'_i \exp\left(c \frac{N^{\max}_{up,i}}{N^{\max}_{up,i-1}}\right) \text{ if } N^{\max}_{up,i} > N^{\max}_{up,i-1}. \quad (14)$$

$N^{\max}_{up,i}$ is the maximum number of crystals E_{up} formed during the isothermal step i. σ' is considered constant once nucleation rates decrease. For the calculations presented in Fig. 12, $\sigma'_1 = 0.016$ J/m^2, and a value of 500 is assigned to the factor c in order to fit our observations best. The change of σ' with T is shown in Fig. 12e. σ' ranges between 0.016 and ca. 0.0164 J/m^2 that results in larger crystal sizes and population size ranges and smaller crystal frequencies compared to the case where $\sigma' = 0.016$ J/m^2 was considered constant during crystallization (Figs. 8a and 12a).

Besides its influence on garnet CSD and chemical composition, perhaps the most dominant influence of σ' is on the departure from equilibrium required to nucleate garnet. There is a linear relationship between ΔG_V and thermal overstep at conditions at which the composition of the equilibrium matrix assemblage does not change (Fig. 7a). However, the relationship between σ' and thermal overstep is rather quadratic (Fig. 13a) following expression (4). It is important to note that the energy barrier to nucleation, $\Delta G^{\star}$, is not constant but increases with σ' (Fig. 13b). The reason that garnet nucleates despite a slightly increased barrier to nucleation are faster diffusion processes at the interface between the matrix and subcritical garnet clusters as T rises. The dashed line in Fig. 13a extends the relationship between thermal overstep and σ' by extrapolation to degrees of disequilibrium not possible in our simulations. It may be used to predict the order of magnitude of apparent interfacial energies during garnet nucleation if mineral reactions in the rock matrix, such as staurolite formation, are kinetically hindered as well. In our simulations, garnet can only nucleate at 3,350 bar if $\sigma' < 0.03$ J/m^2 since higher apparent interfacial energies cannot be counterbalanced by ΔG_V. For any T below the staurolite-in reaction, and for $\sigma' \geq 0.03$ J/m^2, changes to D (see Sect. "The molecular mobility at the garnet-matrix interface, D") or HR (Sect. "The influence of the heating rate, HR, on crystallization kinetics") do not result in the formation of the, respectively, bigger garnet nuclei.

The molecular mobility at the garnet-matrix interface, D

In our simulations, D largely influences crystal sizes and frequencies (Fig. 14) but its impact on overstepping is negligible. Similar to Fig. 13, σ'/overstep relationships were calculated for a series of proportionality factors, k (see expression (13)), that differ by several orders of magnitude. They are identical to the relations illustrated in Fig. 13 and, therefore, are not explicitly shown. These calculations imply that the influence of D on the departure from equilibrium required to nucleate garnet is insignificant compared to the influence of σ'. It also suggests that garnet would not nucleate in 93CW4 if $\sigma' \geq 0.03$ J/m^2 for any value of D at a pressure of 3,350 bar and below the equilibrium temperature of staurolite formation.

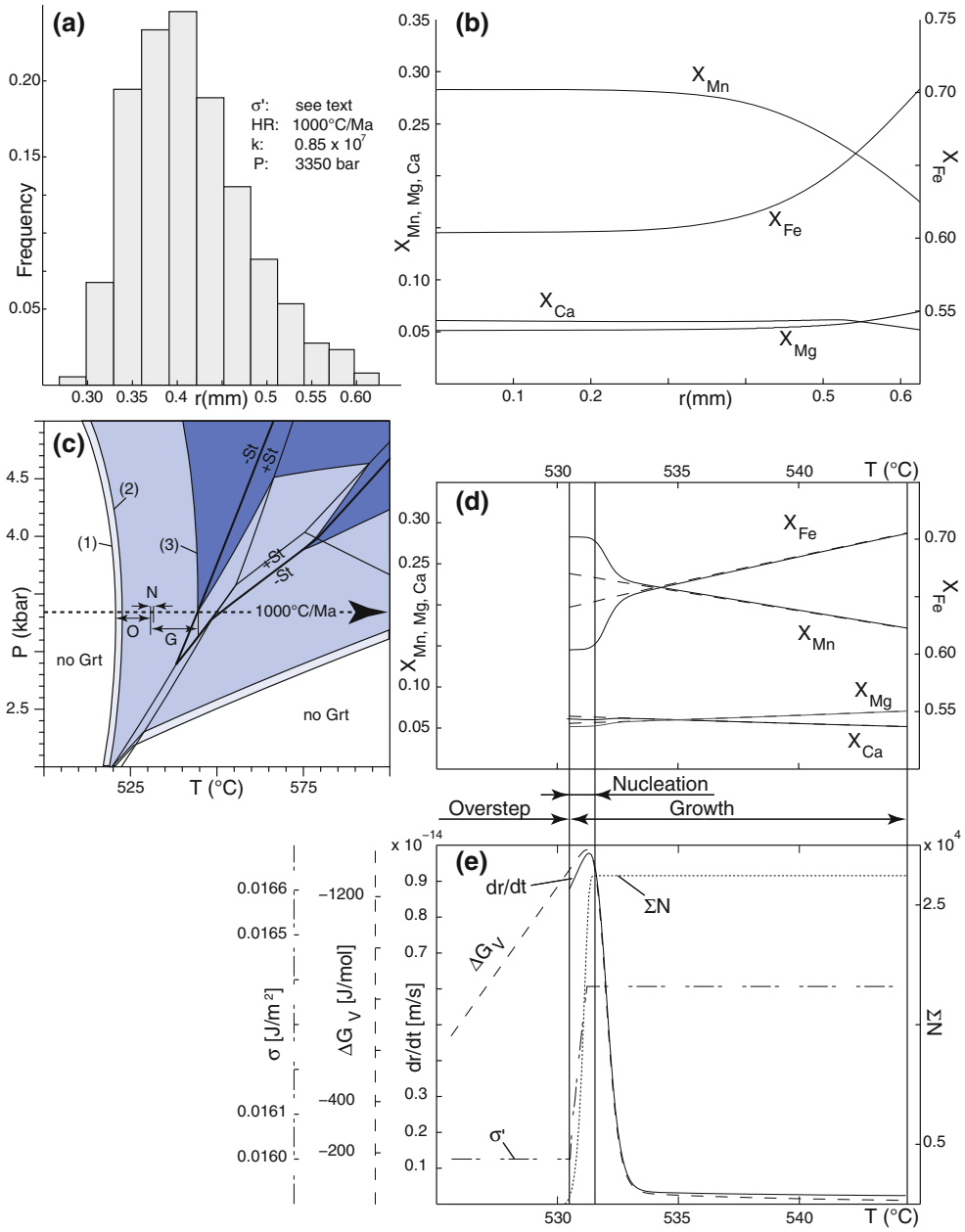

Fig. 12 Like Fig. 8 but with σ' variable

The influence of the heating rate, HR, on crystallization kinetics

Similar to *D*, *HR* largely impacts on growth and nucleation rates (Fig. 15). Its influence on the departure from equilibrium required to nucleate garnet is insignificant. Figure 15 illustrates that crystals get smaller and crystal frequencies increase as *HR* increases. It is interesting to note that the *T* range over which nucleation occurs also depends on *HR*. As the time available for crystal growth decreases with increasing heating rates, the impact of chemical fractionation on garnet stability drops, extending the rates and *T* ranges of nucleation. Our model predicts that there are more variations in the core compositions of a garnet population that crystallizes during fast heating compared to nucleation and growth in the course of slow heating. In general, the impact of chemical fractionation on ΔG_V is primarily dependent on the efficiency of chemical diffusion in garnet relative to the rate with which *T* changes during crystallization. In our simulations, diffusion of Fe, Mn, Ca, and Mg in garnet was insignificant for $HR \geq 500$°C/Ma and, thus, did not result in what Spear (1988) refers to as internal metasomatism. Based on models of heat conduction and the occurrence of isograds in the Nelson aureole, values for *HR* that range between 750 and 1,200°C/Ma were estimated.

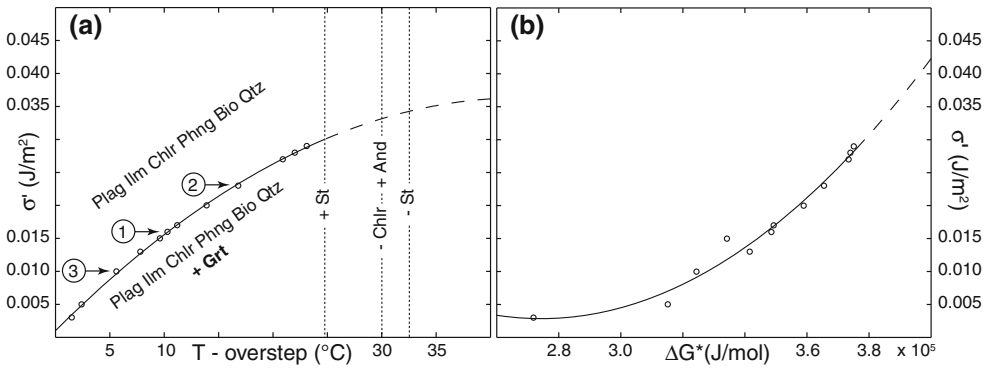

Fig. 13 Relationship between the apparent interfacial energy, σ', and the corresponding departure from equilibrium required to nucleate garnet in 93CW4 at 3,350 bar. *Unbroken curves* reflect quadratic fits to simulation data *marked with circles*. *Dashed curves* are extrapolations to higher degrees of overstep. *Dotted lines* mark the T at which equilibrium phase relations change in the rock matrix. ①, ② and ③ correspond to the cases illustrated in Figs. 8, 9, and 10, respectively. The influence of changes in HR and k on the calculation results are insignificant (see Sects. "The molecular mobility at the garnet-matrix interface, D" and "The influence of the heating rate, HR, on crystallization kinetics")

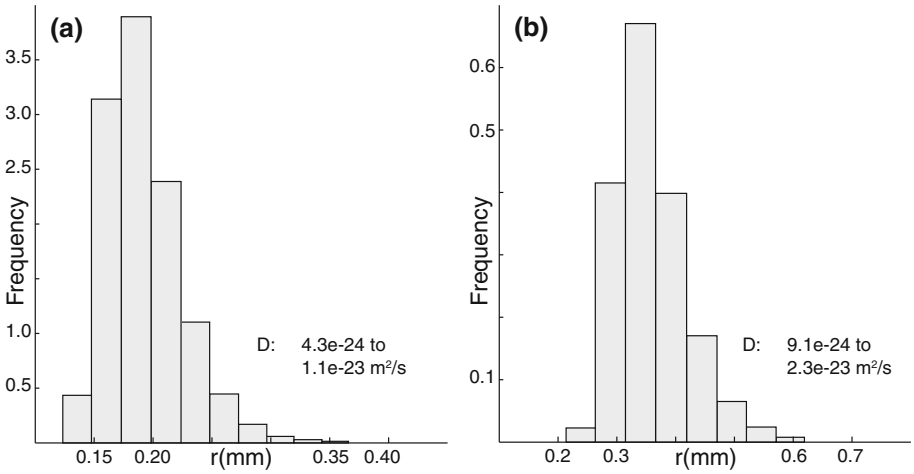

Fig. 14 Influence of D on garnet CSD in rock cylinder of 93CW4. $\sigma' = 0.016$ J/m^2, $HR = 1{,}000$ °C/Ma, $P =$ 3,350 bar. *Lower* and *upper limits* of D reflect changes in T during crystallization. **a** $k = 0.7 \times 10^7$, **b** $k = 1.5 \times 10^7$

Crystallization at different pressures, P

The results presented so far were obtained for $P = 3{,}350$ bar (Figs. 8, 9, 10, 11, 12, 13, 14, 15). Even though phase assemblages with garnet may be thermodynamically stable down to $P \approx$ 2,000 bar (Fig. 6), the probability that garnet nucleates significantly decreases as P drops. The lower limits of staurolite and andalusite stability, which mark the "channel" in $\Delta G_V - P - T$ space (Fig. 6), shift to lower T as P decreases so that the T range of garnet nucleation shrinks. In addition, the maximum Gibbs free energy that can be dissipated during garnet nucleation decreases (ΔG_V gets more positive) as P decreases. This is the reason why garnet does not nucleate at $P = 2{,}350$ bar if $\sigma' \geq 0.015$ J/m^2, whereas it does nucleate at $P = 4{,}350$ bar unless $\sigma' \geq 0.042$ J/m^2. The upper limit of σ' above which nucleation of garnet is predicted not to happen in 93CW4, σ'_{max}, is illustrated in Fig. 16 relative to P.

Discussion

Our simulations suggest that crystal sizes and abundances that result from interface-controlled crystallization are very sensitive to variations in σ', D, HR, and P. The determination of any of these variables from the characteristics of a CSD is ambiguous if the others are unknown. Based on phase equilibria and thermal modeling and detailed petrography of metapelites from the Nelson aureole, Pattison and Tinkham (2009) derived a P of ca. 3,500 bar during contact metamorphism. As the garnet and staurolite isograds are almost coincident in the Nelson aureole (Fig. 15a of Pattison and Tinkham 2009), and considering the simplifications of the model presented in this study, a P of 3,500 bar may correspond to a maximum value of $\sigma' = 0.03$ J/m^2 (Fig. 16). Even if a large departure from equilibrium was required to nucleate staurolite, values for $\sigma' > 0.045$ are unlikely considering the quadratic relationship between σ' and T - overstep shown in Fig. 13a.

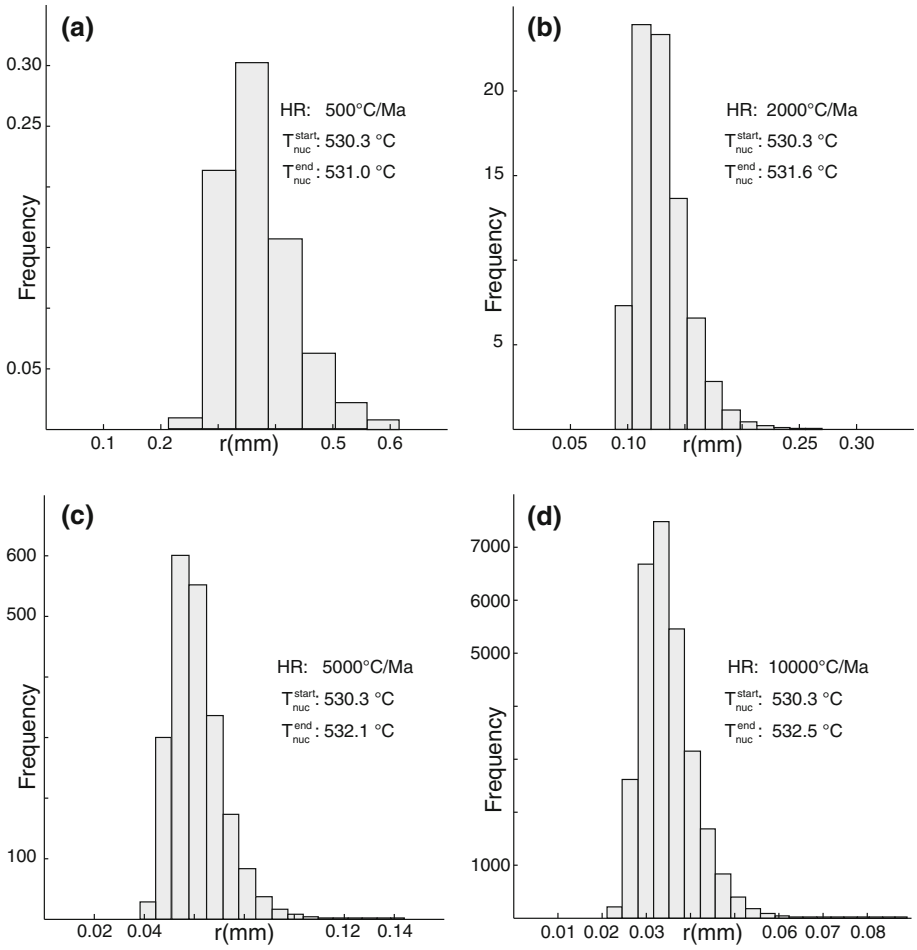

Fig. 15 Influence of heating rate, *HR*, on crystal sizes, crystal frequencies, and the T - range of nucleation in the rock cylinder of 93CW4. $\sigma' = 0.016$ J/m^2, $k = 0.85 \times 10^7$, $P = 3{,}350$ bar

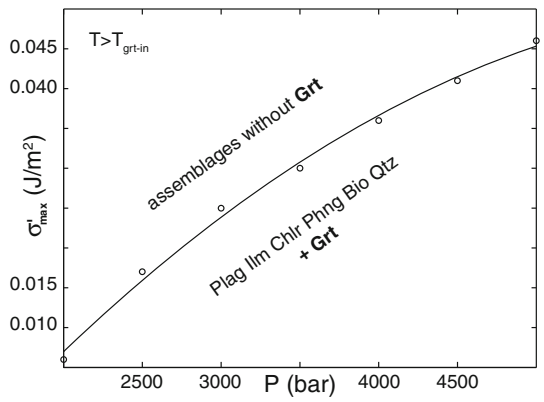

Fig. 16 Relationship between P and σ'_{max}, the maximum apparent interfacial energy above which nucleation of garnet does not happen in 93CW4

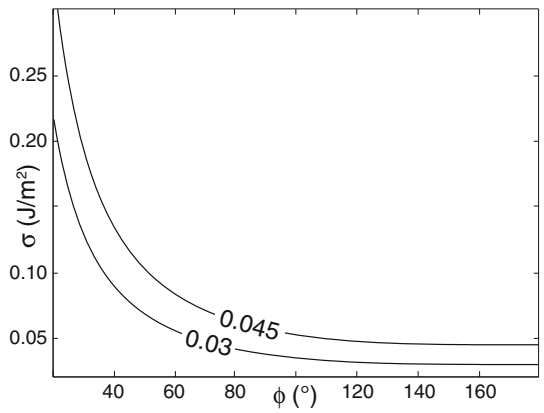

Fig. 17 Relationship between the interfacial energy during heterogeneous nucleation, σ, and the contact angle for nucleation on a planar substrate, ϕ, based on the apparent interfacial energies $\sigma' = 0.03$ and 0.045 J/m^2

Figure 17 illustrates the relationship between σ and the contact angle, ϕ, for $\sigma' = 0.03$ and 0.045 J/m^2 assuming garnet nucleation on a planar matrix substrate (see expression (6)). If $\phi = 180°$, σ equals σ' as this corresponds to homogeneous nucleation. For $\phi < 180°$, the contribution of σ to the energy barrier that has to be overcome in order to nucleate garnet decreases due to the presence of heterogeneities. Since ϕ is unconstrained with respect to metamorphic garnet nucleation, our simulations cannot yield a specific value but rather an upper limit for σ that ranges between 0.03 and 0.3 J/m^2.

Garnet isopleth geothermobarometry (e.g., Vance and Mahar 1998; Evans 2004; Gaidies et al. 2006) applied to

the core of the biggest garnet in the cylinder of 93CW4 (sps-alm-prp-grs: 31.4-56.0-6.7-5.9 mol-%, respectively) yields an area of isopleth intersection at T conditions below the lower limit of garnet stability. This apparent discrepancy may be due to (1) uncertainties of the thermodynamic data, (2) an effective bulk rock composition that does not correspond to the bulk composition of 93CW4, or (3) subsequent alteration of the primary garnet core composition. However, it is important to note that a solution phase that crystallizes far from equilibrium most likely has a chemical composition that cannot be predicted by equilibrium principles. Our model takes into account the departure from equilibrium required for crystallization. It predicts the observed core composition only if garnet nucleates and coexists with plagioclase, ilmenite, biotite, white mica, quartz, and andalusite at ca. 2,500 bar and 525°C after a thermal overstep of ca. 15°C (Fig. 6). Nucleation of garnet with the observed core composition may only be possible during isobaric heating if σ' decreased from $\sigma' \geq 0.018$ J/m^2 at T below the andalusite-in to $\sigma' \leq 0.011$ J/m^2 at the onset of garnet nucleation. If σ' would have been constant or even increased with T before crystallization, garnet nucleation, if at all, would have occurred prior to andalusite formation. Such a garnet would have been lower in spessartine and higher in almandine content compared to the observed crystal. A possible decrease in σ' with T is compatible with results obtained by Gutzow et al. (1985). However, a P of 2,500 bar during garnet crystallization is unlikely as this is not consistent with the absence of cordierite and the presence of staurolite in the Nelson aureole (Pattison and Tinkham 2009).

Limitations of the nucleation and growth model

The comparatively simple CNT was chosen in this study as the foundation of the crystallization model for the reason that quantitative models of nucleation during metamorphic petrogenesis are generally lacking. Despite its inherent simplicity, our model may provide a useful understanding of some fundamental physical properties and mechanism that govern interface-controlled nucleation during metamorphism. However, as CNT was developed for crystals nucleating from a melt or aqueous solution, numerous limitations can be expected when applied to nucleation in metamorphic rocks. This section focuses on some of the major limitations of CNT applied to metamorphic nucleation.

Since CNT is an interface-controlled theory, its application to rocks with relatively slow element transport rates and local variations in ΔG_V is limited. In order to overcome these limitations, alternative quantitative models are required that take into account the influence of long-range diffusion on nucleation kinetics. Whereas such models were successfully developed to predict, for example, the kinetics of oxygen precipitation in Czochralski-grown silicon (Kelton 2003; Wei et al. 2000), they are currently not available to study diffusion-controlled nucleation during petrogenesis.

It can be expected that garnet nuclei are characterized by different volumes and shapes than the rock matrix phases they replace during metamorphism. This is the reason why elastic strain energy may significantly impact on the kinetics of garnet nucleation. In addition, it may be speculated that Gibbs free energy stored in the rock matrix in the form of strained crystals may be released during thermal overstepping and, thus, reduce the amount of ΔG_V required to counterbalance σ'. Such a scenario could not be considered in our simulations of contact metamorphism due to the intrinsic limitations of CNT. However, it can be expected that the release of strain energy is key to the kinetics of garnet nucleation during regional metamorphism.

Besides its interface control and the exclusion of elastic strain energy, the major limitation of CNT is the "capillarity approximation": ΔG_V and σ' are assumed to have macroscopic values independent of cluster size. In our simulations, more than 100 molecules were calculated to be contained in the smallest nuclei. This demonstrates that macroscopic properties were not assigned to embryo sizes and that the clusters are distinguishable from the equilibrium solution (Kelton et al. 1983). According to CNT, in our simulations, molecules of garnet are assumed to be present in the matrix once $\Delta G_V < 0$, and it is further assumed that these molecules eventually form nuclei with a well-defined volume and surface area. However, it seems more likely that metamorphic nucleation takes place along grain boundaries, dislocations, and cracks so that nuclei geometries are rather irregular.

In our model, ΔG_V is not only the chemical driving force for nucleation but it is also used as the driving force for crystal growth (see expression (12)). However, chemical potential differences at the garnet-matrix interface are required for trans-interface interdiffusion driving crystal growth (Hillert 1999; Hillert and Rettenmayr 2003) (i.e., $\Delta\mu^A$ must be different from $\Delta\mu^B$ in Fig. 5). This is not considered in our simulations due to the lack of detailed information on interface kinetics during metamorphism. It is also important to note that our model considers an energy barrier to nucleation but does not account for an energy barrier to crystal growth. As a consequence, preexisting clusters with $r > r^\star$ grow if $\Delta G_V < 0$ independent of $\Delta G^\star$. Both a too large driving force for crystal growth and the omission of an energy barrier to crystal growth result in the overestimation of chemical fractionation and its impeding impact on nucleation. This is the reason for the small T - ranges over which nucleation took place in our simulations and explains the similarities in the core compositions

of all the crystals of a garnet population predicted by our model. It is important to note that this prediction is inconsistent with the garnet cores observed in 93CW4 which decrease with decreased size in X_{Mn} and X_{Ca} and increase in X_{Fe} and X_{Mg}, respectively (see Fig. 5 of Pattison and Tinkham 2009). This also implies that the shapes of the CSDs and the relative crystal sizes and frequencies predicted by our model are more relevant for the interpretation of nucleation and crystal growth kinetics than absolute numerical values.

Conclusions

The model presented in this study reproduces the characteristic lognormal shape of the observed garnet CSD. Since this type is among the most common types of CSDs observed in igneous, sedimentary and metamorphic rocks (Eberl et al. 1998), the model may reflect some course realism despite its intrinsic simplicity. The model results imply that there is a positive relationship between thermal overstep and σ for isobaric garnet nucleation. If the corresponding P is known, σ may be approximated. For garnet nucleation on a planar matrix substrate in the Nelson aureole at 3,500 bar and contact angles between 20 and 180°, σ may range from 0.03 to 0.3 J/m^2. It may be postulated that thermal overstepping of the garnet-forming reaction is larger during fast low—P contact metamorphism than in regional metamorphic settings with slow heating rates. Our simulations suggest that such a phenomenon may be due to relatively small chemical driving forces for garnet nucleation at low P and a limited input of strain energy released during precursor dissolution rather than fast heating as this has a negligible effect on overstepping.

The model presented in this study is the first quantitative attempt at *ab initio* modeling of metamorphic reaction kinetics and may provide grounds for a more complete treatment. Quantitative models that link attachment and detachment processes at the surfaces of product clusters with long-range element transport and strain evolution during crystallization are required to develop a general picture of the kinetics of metamorphic nucleation and crystal growth. Even though the interfacial energy is small compared to the volumetric Gibbs free energy that is released during mineral reactions, this study has clearly shown that knowledge of its magnitude is essential for a better understanding of rock texture formation.

Acknowledgments This paper benefited from critical comments and suggestions by Frank Spear, Bill Carlson, and an anonymous reviewer and the editorial handling of Jochen Hoefs. Benita Putlitz and Lukas Baumgartner are thanked for their help with XR-CT, Willy Tschudin for the help with the sample preparation, Peter Jones, David Moynihan, and Rob Marr for their help with EPMA, and Jean-Claude Lavanchy for the XRF analysis. This research was supported by SNF Research Grant PBBS2-120550 to F.G., and NSERC Research Grant 037233 to D.P.

References

Becker R, Döring W (1935) Kinetische Behandlung der Keimbildung in übersättigten Dämpfen. Annalen der Physik 24:719–752

Carlson WD (1989) The significance of intergranular diffusion to the mechanism and kinetics of porphyroblast crystallization. Contrib Mineral Petrol 103:1–24

Carlson WD (1991) Competitive diffusion-controlled growth of porphyroblasts. Mineral Mag 55:317–330

Carlson WD (2011) Porphyroblast crystallization: linking processes, kinetics, and microstructures. Int Geol Rev 53:406–445

Carlson WD, Denison C, Ketcham RA (1995) Controls on the nucleation and growth of porphyroblasts: kinetics from natural textures and numerical models. Geol J 30:207–225

Cashman KV, Ferry JM (1988) Crystal size distribution (CSD) in rocks and the kinetics and dynamics of crystallization. 3. Metamorphic crystallization. Contrib Mineral Petrol 99:401–415

Chakraborty S, Ganguly J (1992) Cation diffusion in aluminosilicate garnets: experimental determination in spessartine-almandine diffusion couples, evaluation of effective binary, diffusion coefficients, and applications. Contrib Mineral Petrol 111:74–86

Christian JW (1975) The theory of transformations in metals and alloys: Part 1—Equilibrium and general kinetic theory. Pergamon Press, Oxford

de Capitani C, Brown TH (1987) The computation of chemical equilibrium in complex systems containing non-ideal solutions. Geochim Cosmochim Acta 51:2639–2652

de Capitani C, Petrakakis K (2010) The computation of equilibrium assemblage diagrams with Theriak/Domino software. Am Miner 95:1006–1016

Denison C, Carlson WD (1997) Three-dimensional quantitative textural analysis of metamorphic rocks using high-resolution computed X-ray tomography: Part II. Application to natural samples. J Metamorph Geol 15:45–57

Denison C, Carlson WD, Ketcham RA (1997) Three-dimensional quantitative textural analysis of metamorphic rocks using high-resolution computed X-ray tomography: Part I. Methods and techniques. J Metamorph Geol 15:29–44

Eberl DD, Drits VA, Srodon J (1998) Deducing growth mechanisms for minerals from the shapes of crystal size distributions. Am J Sci 298:499–533

Evans TP (2004) A method for calculating effective bulk composition modification due to crystal fractionation in garnet-bearing schist: implications for isopleth thermobarometry. J Metamorph Geol 22:547–557

Florence FP, Spear FS (1991) Effects of diffusional modification of garnet growth zoning on P-T path calculations. Contrib Mineral Petrol 107:487–500

Gaidies F, Abart R, de Capitani C, Schuster R, Connolly JAD, Reusser E (2006) Characterization of polymetamorphism in the Austroalpine basement east of the Tauern Window using garnet isopleth thermobarometry. J Metamorph Geol 24:451–475

Gaidies F, de Capitani C, Abart R (2008) THERIA_G: a software program to numerically model prograde garnet growth. Contrib Mineral Petrol 155:657–671

Ghosh DK (1995) U-Pb geochronology of Jurassic to early Tertiary granitic intrusives from the Nelson-Castlegar area, southeastern British Columbia, Canada. Can J Earth Sci 32:1668–1680

Gibbs JW (1928) The collected works, vol. 1 Thermodynamics. Longmans & Green, New York

Gutzow I, Kashchiev D, Avramov I (1985) Nucleation and crystallization in glass-forming melts: old problems and new questions. J Non Cryst Solids 73:477–499

Hillert M (1999) Solute drag, solute trapping and diffusional dissipation of Gibbs energy. Acta Mater 47:4481–4505

Hillert M (2008) Phase equilibria, phase diagrams and phase transformations: their thermodynamic basis, 2nd Edn. Cambridge University Press, Cambridge

Hillert M, Rettenmayr M (2003) Deviation from local equilibrium at migrating phase interfaces. Acta Mater 51:2803–2809

Holland TJB, Powell R (1998) An internally consistent thermodynamic data set for phases of petrological interest. J Metamorph Geol 16:309–343

Kaischew R, Stranski IN (1934) Concerning the mechanism of the equilibrium of small crystals. Zeitschrift für Physikalische Chemie-Abteilung B-Chemie der Elementarprozesse Aufbau der Materie 26:312–316

Kelton KF (1991) Crystal nucleation in liquids and glasses. In: Ehrenreich H, Turnbull D (eds) Solid state physics. vol. 45. Academic Press, London, pp 75–178

Kelton KF (2000) Kinetic model for nucleation in partitioning systems. J Non Cryst Solids 274:147–154

Kelton KF (2003) Diffusion-influenced nucleation: a case study of oxygen precipitation in silicon. Phil Trans R Soc Lond A 361:429–446

Kelton KF (2006) Nucleation. In: Buschow KH, Cahn RW, Flemings MC, Ilschner B, Kramer EJ, Mahajan S, Veyssiere P (eds) Encyclopedia of materials: science and technology, vol. 7. Elsevier, Amsterdam, pp 6388–6393

Kelton KF, Greer AL, Thompson CV (1983) Transient nucleation in condensed systems. J Chem Phys 79:6261–6276

Kelton KF, Weinberg MC (1994) Calculation of macroscopic growth rates from nucleation data. J Non Cryst Solids 180:17–24

Ketcham RA (2005) Computational methods for quantitative analysis of three-dimensional features in geological specimens. Geosphere 1:32–41

Kretz R (1974) Some models for the rate of crystallization of garnet in metamorphic rocks. Lithos 7:123–131

Kretz R (1993) A garnet population in Yellowknife schist, Canada. J Metamorph Geol 11:101–120

Kubena J, Kubena A, Caha O, Mikulik P (2007) Development of oxide precipitates in silicon: calculation of the distribution function of the classical theory of nucleation by a nodal-points approximation. J Phys Condens Matter 19:496202

Lasaga AC (1998) Kinetic theory in the earth sciences. Princeton University Press, Princeton

Loomis TP, Ganguly J, Elphick SC (1985) Experimental determinations of cation diffusitivities in aluminosilicate garnets. II. Multicomponent simulation and tracer diffusion coefficients. Contrib Mineral Petrol 90:45–51

Pattison DRM, de Capitani C, Gaidies F, (in print) Petrologic consequences of variations in metamorphic reaction affinity. J Metamorph Geol

Pattison DRM, Tinkham DL (2009) Interplay between equilibrium and kinetics in metamorphism of pelites in the Nelson aureole, British Columbia. J Metamorph Geol 27:249–279

Pattison DRM, Vogl JJ (2005) Contrasting sequences of metapelitic mineral-assemblages in the aureole of the tilted Nelson Batholith, British Columbia: Implications for phase equilibria and pressure determination in andalusite-sillimanite-type settings. Can Mineral 43:51–88

Porter DA, Easterling KE (1992) Phase transformations in metals and alloys, 2nd Edn. Chapman and Hall, London

Sevigny JH, Parrish RR (1993) Age and origin of Late Jurassic and Paleocene granitoids, Nelson Batholith, southern British Columbia. Can J Earth Sci 30:2305–2314

Shampine LF, Reichelt MW (1997) The MATLAB ode suit. SIAM J Sci Comput 18:1–22

Shampine LF, Reichelt MW, Kierzenka JA (1999) Solving index-I DAEs in Matlab and Simulink. SIAM Rev 41:538–552

Spear FS (1988) Metamorphic fractional crystallization and internal metasomatism by diffusional homogenization of zoned garnets. Contrib Mineral Petrol 99:507–517

Spear FS (1993) Metamorphic phase equilibria and pressure-temperature-time paths. Mineralogical Society of America Monograph. Mineralogical Society of America, Washington, DC

Spear FS, Daniel CG (1998) Three-dimensional imaging of garnet porphyroblast sizes and chemical zoning: nucleation and growth history in the garnet zone. Geol Mater Res 1:1–44

Thompson CV, Spaepen F (1983) Homogeneous crystal nucleation in binary metallic melts. Acta Metall 31:2021–2027

Tomkins HS, Pattison D (2007) Accessory phase petrogenesis in relation to major phase assemblages in pelites from the Nelson contact aureole, southern British Columbia. J Metamorph Geol 25:401–421

Turnbull D (1950) Formation of crystal nuclei in liquid metals. J Appl Phys 21:1022–1028

Turnbull D, Fisher JC (1949) Rates of nucleation in condensed systems. J Chem Phys 17:71–73

Vance D, Mahar E (1998) Pressure-temperature paths from P-T pseudosections and zoned garnets: potential, limitations and examples from the Zanskar Himalaya, NW India. Contrib Mineral Petrol 132:225–245

Vehkamäki H (2006) Classical nucleation theory in multicomponent systems. Springer, Berlin Heidelberg New York

Volmer M, Weber A (1926) Keimbildung in übersättigten Gebilden. Zeitschrift für Physikalische Chemie 119:277–301

Wei PF, Kelton KF, Falster R (2000) Coupled-flux nucleation modeling of oxygen precipitation in silicon. J Appl Phys 88:5062–5070